2010 American Control Conference
Marriott Waterfront, Baltimore, MD, USA
June 30-July 02, 2010

Near-Hover Dynamics and Attitude Stabilization of an Insect Model

B. Cheng and X. Deng

Abstract—**In this paper, we present a mathematical model of near-hover attitude dynamics and control in flapping flight. Then we apply this model to fruit fly (*Drosophila*) as an example. The attitude dynamics are derived from the complete 6-DOF equations of motion. Stability derivatives are estimated based on quasi-steady aerodynamic models of Flapping counter-torques (FCTs). Control derivatives are derived in a similar manner. Results show that stable angular motions can be achieved using a simple proportional feedback control. A coupled yaw and roll rotation (similar to a banked turn) is indentified as the most stable mode of angular motion. Additionally, free response results suggest that the fruit fly is able to damp out an initial disturbance of angular velocity.**

I. Introduction

Recent studies on the stability of insect flight showed that both longitudinal [1-4] and lateral [5] dynamics are inherently unstable. For example, it has been shown that a particular coupling of pitching and forward motion causes the instability during both hovering [1] and forward flight [4]. Moreover, even with static control responses, no asymptotic longitudinal stability was found for tethered locust *Schistocerca gregaria* [3].

More recent studies found that due to a passive mechanism known as flapping counter-torque (FCT), insect flight subjects to an inherent damping of angular velocity about roll, pitch [6] and yaw [7-9] axes of rotation. Remarkably, the damping is sufficient to decelerate the body yaw rotation at a rate observed in free flight maneuvers for different size scales of flapping wing flies [9].

In this study, we first derived a stroke-averaged 6-DOF model for flapping-wing insects based on the flapping counter-torque [6, 7, 9] and flapping counter-force (FCF) models. Then we studied the near-hover attitude dynamics and control of a model insect (mimicking the morphology and wing kinematics of fruit fly *Drosophila*) assuming zero translational velocities. Closed-loop dynamics were obtained using three independent control inputs. In addition, under open loop conditions, we simulated the responses of the system due to different initial disturbances.

II. Insect Flight Modeling

Head, thorax and abdomen of the model insect are modeled as three rigid ellipsoids (Fig. 1) based on the morphological data of fruit fly *Drosophila* (Appendix C in [8]). We first consider the insect body oriented with a fixed pitch angle χ_0 (free body angle) relative to a horizontal stroke plane (Fig. 1). The stroke plane frame is fixed to the body with the origin located at the wing base. We define the body frame (x_b, y_b, z_b) having the same orientation with the stroke plane frame, but with the origin located at the center of gravity. The distance between the wing base and the center of gravity is specified by l_1 .The moment of inertia matrix relative to the body frame is calculated as:

$$\mathbf{I}_b = \begin{bmatrix} I_{xx} & 0 & -I_{xz} \\ 0 & I_{yy} & 0 \\ -I_{zx} & 0 & I_{zz} \end{bmatrix} = \begin{bmatrix} 0.3058 & 0 & -0.1913 \\ 0 & 0.5060 & 0 \\ -0.1913 & 0 & 0.3058 \end{bmatrix} \times 10^{-12}\,\mathrm{N\,m\,s^2} \quad (1)$$

The wing kinematics are modeled with two degrees of freedom: a stroke angle $\phi(t)$ equals to $(\Phi/2)\sin(2\pi nt)$ and a rotation angle $\psi(t)$ equals to $(\Psi/2)\cos(2\pi nt)$; where the stroke amplitude (Φ), maximum rotation angle (Ψ) and flapping frequency (n) are selected at 130º, 60º and 212 Hz, which are close to the measured values in free flying fruit flies [10]. The instant angle of attack $\alpha(t)$ is calculated by $\pi/2 - \psi(t)$. Note that stroke deviation is neglected for simplification purpose.

III. Equations of Motion

A. Linearized flight dynamics during hover

The complete dynamics of a rigid body are described by the Newton-Euler equations [11], which comprise six equations with translational velocity (u, v, w) and angular velocity (p, q, r) as unknowns. With the addition of another six kinematic equations describing the body position (x, y, z) and orientation (ϕ, θ, ψ) relative to the Earth-fixed frame, a complete system of equations includes twelve coupled nonlinear ordinary differential equations. The aerodynamic forces (X, Y, Z) and

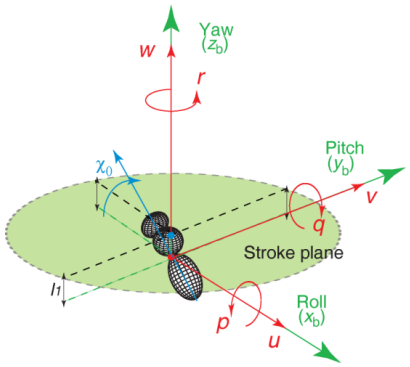

Fig. 1. A schematic view of the body coordinate frame (x_b, y_b, z_b). The body frame is originated at the center of gravity (red dot), which is located below the wing base (blue dot). The distance between the center of gravity and the wing base is specified by l_1. The translational velocity components (u, v, w) and angular velocity components (p, q, r) are defined about the x_b, y_b, and z_b axes, respectively.

This work was supported in part by NSF Grant#0545931. The School of Mechanical Engineering, Purdue University, Email: xdeng@purdue.edu.

torques (L, M, N), acting along or around the body axes [3], are incorporated in these equations. To analyze the near-hover flight dynamics, we linearize the equations of motion using small perturbation theory. We first assume the reference flight condition of hovering:

$$p_e = q_e = r_e = u_e = v_e = w_e = \theta_e = \phi_e = 0, \quad (2)$$

and the aerodynamic forces and torques are zero in the equilibrium state. Then we approximate the aerodynamic forces and torques as stroked-averaged analytical functions of the perturbed motion variables (i.e., stability derivatives multiplied by the corresponding disturbance quantity of the motion variables, for details refer to [3]). A complete description of this method can be found in [12]. Therefore, we have:

$$\dot{\mathbf{x}} = \mathbf{A} + \mathbf{x} + \Delta(\mathbf{x}) \quad (3)$$

$$\mathbf{A} = \begin{bmatrix} \frac{X_u}{m} & 0 & 0 & g & 0 & 0 & 0 & 0 \\ 0 & \frac{Z_w}{m} & 0 & 0 & 0 & 0 & 0 & 0 \\ C_3M_u & 0 & C_3M_q & 0 & 0 & 0 & 0 & 0 \\ 0 & 0 & 1 & 0 & 0 & 0 & 0 & 0 \\ 0 & 0 & 0 & 0 & \frac{Y_v}{m} & 0 & 0 & -g \\ 0 & 0 & 0 & 0 & C_4L_v & C_4L_p & C_1N_r & 0 \\ 0 & 0 & 0 & 0 & C_1L_v & C_1L_p & C_2N_r & 0 \\ 0 & 0 & 0 & 0 & 0 & 1 & 0 & 0 \end{bmatrix} \quad (4)$$

where $\mathbf{x} = (u, w, q, \theta, v, p, r, \phi)^T \in R^8$, C_1, C_2, C_3 and C_4 are constants of body moment of inertia:

$$C_1 = \frac{I_{xz}}{I_{xx}I_{zz} - {I_{xz}}^2}$$
$$C_2 = \frac{I_{xx}}{I_{xx}I_{zz} - {I_{xz}}^2}$$
$$C_3 = \frac{1}{I_{yy}}$$
$$C_4 = \frac{I_{zz}}{I_{xx}I_{zz} - {I_{xz}}^2} \quad . \quad (5)$$

Because body position (x, y, z) and head angle ψ do not affect the aerodynamic steady state, they can be considered separately with appropriated equations [12]. In Eqn. 4, X_u, Y_v, Z_w, L_p, M_q, N_r, L_v and M_u are the only non-zero stability derivatives due to the simplifications made in the current study. $\Delta(\mathbf{x})$ represents the modeling uncertainties which include the errors from averaging, linearization process and approximation of aerodynamic forces and torques.

B. Attitude dynamics with wing asymmetries

The attitude dynamics are reduced from the complete 6-DOF flight dynamics described by Eqn. 4. In general, the attitude dynamics are coupled with the translational velocities (as shown in Eqn. 4). In the current study, we assume the flight dynamics are limited to the 3-DOF angular motions; therefore there is no effect of translational velocity on aerodynamic moments. This can be illustrated by considering the model insect tethered at its center of gravity by a universal joint fixed to the Earth, eliminating any translational component of velocity.

Observed from free-flying insects [10, 13, 14], we choose the following wing asymmetries as the control variables to stabilize the attitude: 1) $\Delta\Phi$: differential change of stroke amplitudes for left and right wings (Fig. 2A), which is designed to modulate roll torque L; 2) equal change of mean stroke angle $\bar{\Phi}$ for left and right wings (Fig. 2B), which is designed to modulate pitch torque M; 3) $\Delta\Theta$: differential change of stroke plane tilt angles for left and right wings (Fig. 2C), which is designed to modulate yaw torque N. The partial derivatives of aerodynamic torques (L, M, N) with respect to the control variables are known as control derivatives, the estimations of which are described in Section IV.

Now, we write the attitude dynamics incorporating the control inputs as:

$$\dot{\mathbf{x}}_\mathrm{a} = \mathbf{A}_\mathrm{a}\mathbf{x}_\mathrm{a} + \mathbf{B}_\mathrm{a}\mathbf{c} \quad (6)$$

where $\mathbf{x}_\mathrm{a} = [p \quad q \quad r \quad \phi \quad \theta \quad \psi]^\mathrm{T} \in R^6$ is state vector and $\mathbf{c} = [\Delta\Phi \quad \Delta\Theta \quad \bar{\Phi}]^\mathrm{T}$ is control vector; $\mathbf{A}_\mathrm{a}$ is system matrix:

$$\mathbf{A}_\mathrm{a} = \begin{bmatrix} C_4L_p & 0 & C_1N_r & 0 & 0 & 0 \\ 0 & C_3M_q & 0 & 0 & 0 & 0 \\ C_1L_p & 0 & C_2N_r & 0 & 0 & 0 \\ 1 & 0 & 0 & 0 & 0 & 0 \\ 0 & 1 & 0 & 0 & 0 & 0 \\ 0 & 0 & 1 & 0 & 0 & 0 \end{bmatrix} \quad (7)$$

and $\mathbf{B}_\mathrm{a}$ is control system matrix:

$$\mathbf{B}_\mathrm{a} = \begin{bmatrix} C_4L_{\Delta\Phi} & C_1N_{\Delta\Theta} & 0 \\ 0 & 0 & C_3M_{\bar{\Phi}} \\ C_1L_{\Delta\Phi} & C_2N_{\Delta\Theta} & 0 \\ 0 & 0 & 0 \\ 0 & 0 & 0 \\ 0 & 0 & 0 \end{bmatrix}. \quad (8)$$

IV. Stability and Control Derivatives

A. Estimation of stability derivatives

The stability derivatives can be estimated based on FCT and FCF models (refer to Appendix A), which describe the aerodynamic counter-torques/forces generated by a wing pair during rotations/translations about roll, pitch and yaw axes. Based on quasi-steady aerodynamic models, analytical estimations are developed.

Table 1 summarizes the non-zero stability derivatives associated with flight dynamics during hover. Note L_v (M_u) equals Y_v (X_u) times the distance between the wing base and the center of gravity l_1. Other stability derivatives are expected to be zero (e.g., X_v, N_p) since FCTs and FCFs act collinear with the rotating/translating axes. It is important that we assumed the near-hover condition, which leaves the lift and drag coefficients dependent on only the angle of attack (eliminating the effect of translational velocity on the aerodynamics). Now, the stability derivatives are ready to be

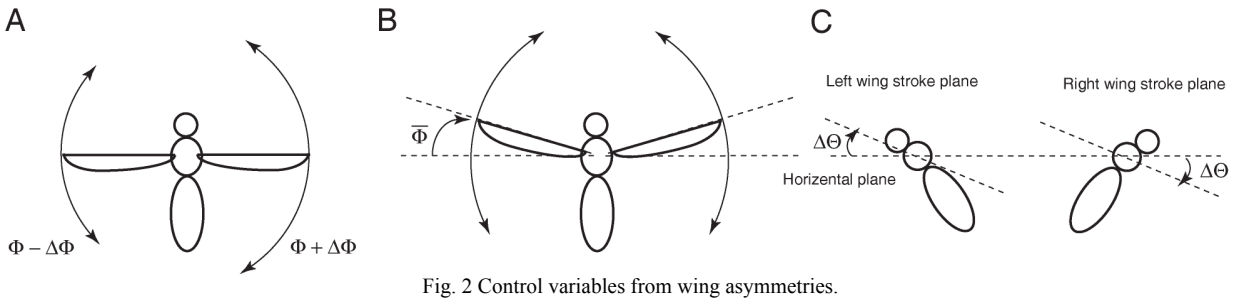

Fig. 2 Control variables from wing asymmetries.

calculated with proper morphological and wing kinematic data.

Table 1. Analytical estimations of stability derivatives with non-zero values.

Stability Derivatives		Analytical estimations
X_u	$\overline{\frac{f_{roll}}{u}}$	$-\rho R^2 \bar{c} \hat{r}_1^1(S) \Phi n \overline{C_D(\alpha_0) \cos^2(\phi) \left\lvert \frac{d\hat{\phi}}{d\hat{t}} \right\rvert}$
Y_v	$\overline{\frac{f_{pitch}}{v}}$	$-\rho R^2 \bar{c} \hat{r}_1^1(S) \Phi n \overline{C_D(\alpha_0) \sin^2(\phi) \left\lvert \frac{d\hat{\phi}}{d\hat{t}} \right\rvert}$
Z_w	$\overline{\frac{f_{yaw}}{w}}$	$-\frac{1}{2} \rho R^2 \bar{c} \hat{r}_1^1(S) \Phi n \overline{\frac{dC_L(\alpha)}{d\alpha}_{\lvert \alpha=\alpha_0} \left\lvert \frac{d\hat{\phi}}{dt} \right\rvert}$
L_p	$\overline{\frac{\tau_{roll}}{p}}$	$-\frac{1}{2} \rho R^4 \bar{c} \hat{r}_2^2(S) \hat{r}_{cp} \overline{\frac{\mathrm{d}C_L(\alpha)}{\mathrm{d}\alpha}_{\lvert \alpha_0} \cos^2(\phi) \left\lvert \frac{d\hat{\phi}}{d\hat{t}} \right\rvert} \Phi n$
M_q	$\overline{\frac{\tau_{pitch}}{q}}$	$-\frac{1}{2} \rho R^4 \bar{c} \hat{r}_2^2(S) \hat{r}_{cp} \overline{\frac{\mathrm{d}C_L(\alpha)}{\mathrm{d}\alpha}_{\lvert \alpha_0} \sin^2(\phi) \left\lvert \frac{d\hat{\phi}}{d\hat{t}} \right\rvert} \Phi n$
N_r	$\overline{\frac{\tau_{yaw}}{r}}$	$-\rho R^4 \bar{c} \hat{r}_2^2(S) \hat{r}_{cp} \Phi \overline{C_D(t) \left\lvert \frac{d\hat{\phi}}{d\hat{t}} \right\rvert} n$
L_v	$\overline{\frac{f_{pitch}}{v}} l_1$	$-\rho R^2 \bar{c} \hat{r}_1^1(S) \Phi n \overline{C_D(\alpha_0) \sin^2(\phi) \left\lvert \frac{d\hat{\phi}}{d\hat{t}} \right\rvert} l_1$
M_u	$\overline{\frac{f_{roll}}{u}} l_1$	$-\rho R^2 \bar{c} \hat{r}_1^1(S) \Phi n \overline{C_D(\alpha_0) \cos^2(\phi) \left\lvert \frac{d\hat{\phi}}{d\hat{t}} \right\rvert} l_1$

$\overline{f_{roll}}$, $\overline{f_{pitch}}$ and $\overline{f_{yaw}}$ denote the FCFs during translations along each principal axis in the body frame; $\overline{\tau_{roll}}$, $\overline{\tau_{pitch}}$ and $\overline{\tau_{yaw}}$ denote the FCTs during rotations about each principal axis in the body frame. $C_L(\alpha)$ and $C_D(\alpha)$ are the lift and drag force coefficients as functions of the angle of attack α [15], α_0 is the geometric angle of attack, ρ is the fluid/air density, R is the wing length, $\bar{c}$ is the mean chord length, $\left(\frac{d\hat{\phi}}{d\hat{t}}\right)$ is the normalized wing angular velocity, Φ and n are the wing flapping amplitude and frequency, $\hat{r}_2(S)$ is the dimensionless second moment of wing area, $\hat{r}_{cp}$ is the dimensionless center of pressure, ϕ is the stroke angle and φ is the wing rotation angle.

B. Estimation of Control Derivatives

Using quasi-steady aerodynamic models [15, 16], in Appendix B, we derive the mathematical estimations of control derivatives, summarized in Table 2. Note that, all the control and stability derivatives are calculated on stroke-by-stroke basis. Remarkably, each wing asymmetry only generates an aerodynamic torque about an individual principal axis, indicating a decoupled control of roll, pitch and yaw moments by $\Delta\Phi$, $\bar{\Phi}$ and $\Delta\Theta$.

Table 2. Analytical estimations of control derivatives with non-zero values.

Control derivatives	Analytical estimations
$L_{\Delta\Phi}$	$\frac{1}{2} \rho R^4 \bar{c} n^2 \hat{r}_2^2(S) \hat{r}_{cp} \Phi \overline{C_L(\alpha) \left(\frac{d\hat{\phi}}{d\hat{t}}\right)^2 \cos(\phi)}$
$M_{\bar{\Phi}}$	$\frac{1}{4} \rho R^4 \bar{c} n^2 \hat{r}_2^2(S) \hat{r}_{cp} \Phi^2 \overline{C_L(\alpha) \left(\frac{d\hat{\phi}}{d\hat{t}}\right)^2}$
$N_{\Delta\Theta}$	$\frac{1}{4} \rho R^4 \bar{c} n^2 \hat{r}_2^2(S) \hat{r}_{cp} \Phi^2 \overline{C_L(\alpha) \left(\frac{d\hat{\phi}}{d\hat{t}}\right)^2}$

C. Estimation errors

The estimations of both stability and control derivatives may subject to errors from the neglected aerodynamic effects (e.g., rotational lift, wake capture and added mass [17]). Experimental results [6] showed that, predictions of roll and yaw FCT models match closely to the measured values, while pitch FCT model tends to underestimate the measured values. Therefore, we expect stability derivative M_q lower than the actual value. On the other hand, experimental results for FCFs as well as control derivatives are still lacking, which need to be studied systematically in the future. Readers can refer to [5, 18] for related studies.

V. Closed Loop Attitude Dynamics

A. Active Stabilization

Due to the inherent flight instability, to achieve stable attitude dynamics, an active control is required to regulate the angular positions. Therefore, based on the estimated mapping from control variables ($\Delta\Phi$, $\bar{\Phi}$, $\Delta\Theta$) to aerodynamic moments (L, M, N) (Table 2), we choose the following control algorithm, which is similar to a Proportional-Derivative (PD) control :

$$\begin{bmatrix} \Delta\Phi \\ \Delta\Theta \\ \bar{\Phi} \end{bmatrix} = \begin{bmatrix} k_1 & 0 & 0 & k_2 & 0 & 0 \\ 0 & 0 & k_5 & 0 & 0 & k_6 \\ 0 & k_3 & 0 & 0 & k_4 & 0 \end{bmatrix} \mathbf{x}_a = \mathbf{K}\mathbf{x}_a, \tag{9}$$

where k_1, k_2, k_3, k_4, k_5 and k_6 are design parameters, which are properly chosen to yield desired stability.

B. Closed Loop Attitude Dynamics

The closed loop attitude dynamics are now ready to be investigated by incorporating Eqn. 9 into Eqn. 6 and then substituting the stability and control derivatives with the corresponding estimations. Collectively, we have:

$$\dot{\mathbf{x}}_a = \mathbf{A}_a^c \mathbf{x}_a \tag{10}$$

where $\mathbf{A}_a^c$ is the closed loop system matrix incorporating the control input $\mathbf{B}_a\mathbf{c}$ in Eqn. 6:

$$\mathbf{A}_a^c = \begin{bmatrix} C_4(L_p + k_1 L_{\Delta\Phi}) & 0 & C_1(N_r + k_5 N_{\Delta\Theta}) & C_4 k_2 L_{\Delta\Phi} & 0 & C_1 k_6 N_{\Delta\Theta} \\ 0 & C_3(M_q + k_3 M_{\dot{\Phi}}) & 0 & 0 & k_4 C_3 M_{\dot{\Phi}} & 0 \\ C_1(L_p + k_1 L_{\Delta\Phi}) & 0 & C_2(N_r + k_5 N_{\Delta\Theta}) & C_1 k_2 L_{\Delta\Phi} & 0 & C_2 k_6 N_{\Delta\Theta} \\ 1 & 0 & 0 & 0 & 0 & 0 \\ 0 & 1 & 0 & 0 & 0 & 0 \\ 0 & 0 & 1 & 0 & 0 & 0 \end{bmatrix} \tag{11}$$

The stability and control derivatives in the matrix are estimated based on analytical estimations presented in Table 1 and 2); C_1, C_2, C_3 and C_4 are calculated based on Eqn. 5.

Next, by applying fruit fly *Drosophila* morphological data [8] and using the wing kinematics described in Section II, we calculate the stability and control derivatives, which are summarized in Table 3 and 4.

Table 3. Stability derivatives

Stability Derivatives	L_p	M_q	N_r
Values (10^{-12} N m s)	-7.55	-3.77	-26.55

Table 4. Control derivatives

Control Derivatives	$L_{\Delta\Phi}$	$M_{\dot{\Phi}}$	$N_{\Delta\Theta}$
Values (10^{-8} N m)	1.22	1.63	1.63

Now we have obtained the system matrix $\mathbf{A}_a^c$, we then calculate its eigenvalues and corresponding eigenvectors by assuming proper values of design parameters (k_1, k_2, k_3, k_4, k_5 and k_6).

It can be seen from Eqn. 9, that k_1, k_3 and k_5 define the magnitudes of feedback from the angular velocity components (p, q, r), and k_2, k_4 and k_6 define the magnitudes of feedback from angular position components (ϕ,θ,ψ). As indicated by [6, 7, 9], flapping-wing flight already subjects to a substantial aerodynamic damping of angular velocities; therefore, we can reduce the PD control to P control by choosing $k_1 = k_3 = k_5 = 0$. In the following, we calculate the system matrix $\mathbf{A}_a^c$ using different values of k_2, k_4 and k_6.

It is easy to see that by choosing negative values of k_2, k_4 and k_6, the stability of the closed-loop system can be ensured, therefore a P control is sufficient to achieve a stable attitude dynamics. For example, choosing $k_1 = k_3 = k_5 = -10^{-4}$ results in an asymptotic stable system of six stable modes with different convergence rates (Table 5). Mode 1, which associates with an in-phase coupling of roll and yaw velocities (similar to a banked turn), is the most stable mode. This might explain why in the nature, insects and birds tend to use banked turns [14] during fast maneuvers. On the other hand, Modes 3, 4 and 6, in which roll, yaw and pitch angles are the dominant variables, have the least stability (slower convergence rates). Therefore, we increase the values of k_2, k_4 and k_6 to enhance the feedback from angular position. Results show that when k_6 is sufficiently large, Modes 5 and 6 (associated with pitch motions) reduced to an oscillatory mode but remains stable. While we further increase the values of k_2 and k_4, Modes 2 and 4, and Modes 1 and 3 also reduce to two separate oscillatory stable modes (e.g., Table 6), and the system consists of three oscillatory stable modes.

Table 5. Eigenvalues and eigenvectors of the system matrix $k_1 = k_3 = k_5 = 0$, $k_2 = k_4 = k_6 = -10^{-4}$

Mode	1	2	3	4	5	6
λ_i	-161.31	-21.67	-0.16	-0.06	-7.00	-0.46
δp	0.59*	-0.98*	0.16*	0	0	0
δq	0	0	0	0	-0.99*	-0.42*
δr	0.80*	0.20*	0	0.06*	0	0
$\delta\phi$	0	0.05	-0.99*	0	0	0
$\delta\theta$	0	0	0	0	0.14*	0.91*
$\delta\psi$	-0.01	-0.01	0	-1.00*	0	0

* dominant variables.

Table 6. Eigenvalues and eigenvectors of the system matrix $k_1 = k_3 = k_5 = 0$, $k_2 = k_4 = k_6 = -1$

Mode	1	2	3
λ_i	-14.05 ± 167.17i	-77.56 ± 343.69i	-3.73 ± 179.44i
δp	0.83*	-0.66 ± 0.07i*	0
δq	0	0	1.0000*
δr	-0.54 ± 0.12i*	-0.74*	0
$\delta\phi$	0	0	0
$\delta\theta$	0	0	-0.00 ∓ 0.01i
$\delta\psi$	0	0	0

* dominant variables.

VI. Simulation of Passive Body Rotation

In a previous study [8], the stability of open-loop attitude dynamics was investigated by looking at the system matrix $\mathbf{A}_a$. The results were inclusive because three zero eginvalues were found for the linearized system. However, the open-loop attitdue dynamics are considered to be unstble because passive damping is at most only able to damp out the angular

velocities, but cannot tune the insect back to the original orientation.

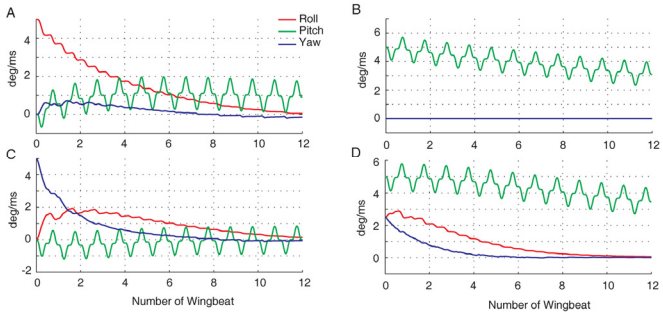

Fig. 3 Simulation results of passive body rotation. Responses to the initial disturbances of angular velocity about A) Roll, B) Pitch, C) Yaw axes, respectively. D) Response to an arbitrary initial disturbance .

To see whether the system is able to damp out arbitrary initial disturbances of angualr velocity, we simulate the attitude dynamics in Matlab enviroment (For details of simulation, refer to [8, 19, 20]). We further assume the dynamics are confined to the 3-DOF angular motions, exculding the aerodynamic effects of translational velocities. The results are summarized in Fig. 3.

It can be seen that initial angular velocities of different types are all damped out in the succeeding motions. And unsprisingly, the damping is strongest about yaw axis.

VII. Conclusions

In this paper, we presented a mathematical model of attitude dynamics and control in insect flight, and used fruit fly (*Drosophila*) as an example. The current model can as well be applied to other flapping-wing insects with specific morphological and wing kinematic data. The results showed that by modulating the magnitude of feedback, different stable flight modes can be achieved. The related future work might include more comprehensive studies on the 6-DOF flight dynamics as well as robotic wing experiments to verify the mathematical estimations of both stability and control derivatives.

Appendix

Based on quasi-steady aerodynamic models [15, 16], we analytically estimate the aerodynamic torques caused by body motions as well as three types of wing asymmetry. For discussion of estimation errors, readers can refer to Section IV, part C.

A. Flapping counter-torques (FCTs) and Flapping counter-forces (FCFs) based on quasi-steady aerodynamic models

Body rotations about the principal axes in the stroke plane frame cause effective wing asymmetries which result in aerodynamic counter torques (FCTs), which can be summarized by the following equations (Readers can refer to [6] for detailed derivations and experimental validations):

$$\overline{\tau_{roll}} \approx -\frac{1}{2}\rho R^4 \bar{c}\hat{r}_2^2(S)\hat{r}_{cp}\overline{\frac{dC_L(\alpha)}{d\alpha}_{|\alpha_0}\cos^2(\phi)\left|\frac{d\hat{\phi}}{d\hat{t}}\right|}\Phi np,$$
$$\overline{\tau_{pitch}} \approx -\frac{1}{2}\rho R^4 \bar{c}\hat{r}_2^2(S)\hat{r}_{cp}\overline{\frac{dC_L(\alpha)}{d\alpha}_{|\alpha_0}\sin^2(\phi)\left|\frac{d\hat{\phi}}{d\hat{t}}\right|}\Phi nq,$$
$$\overline{\tau_{yaw}} = -\rho R^4 \bar{c}\hat{r}_2^2(S)\hat{r}_{cp}\Phi\overline{C_D(t)\left|\frac{d\hat{\phi}}{d\hat{t}}\right|}nr. \quad \text{(A1)}$$

Stroke-averaged FCTs act collinear with the axes of rotation and are linearly dependent on the flapping frequency and angular velocity. Similarly, one can show that the body translations also cause effective wing asymmetries that result in damping forces (FCFs). The FCFs during body translations along body roll (forward/backward), pitch (lateral) and yaw (vertical) axes are calculated:

$$\overline{f_{roll}} = -\rho R^2 \bar{c}\hat{r}_1^1(S)\Phi n\overline{C_D(\alpha_0)\cos^2(\phi)\left|\frac{d\hat{\phi}}{d\hat{t}}\right|}u,$$
$$\overline{f_{pitch}} = -\rho R^2 \bar{c}\hat{r}_1^1(S)\Phi n\overline{C_D(\alpha_0)\sin^2(\phi)\left|\frac{d\hat{\phi}}{d\hat{t}}\right|}v,$$
$$\overline{f_{yaw}} = -\frac{1}{2}\rho R^2 \bar{c}\hat{r}_1^1(S)\Phi n\overline{\frac{dC_L(\alpha)}{d\alpha}_{|\alpha=\alpha_0}\left|\frac{d\phi}{dt}\right|}w, \quad \text{(A2)}$$

respectively.

B. Aerodynamic torque due to wing asymmetries

1) Stroke angle difference:

The lift difference between the left and right wings caused by a stroke angle difference $\Delta\Phi$ will produce a resultant roll moment over a wing stroke (no resultant pitch and yaw moment). The instantaneous magnitude of the lift force produced by a single wing is:

$$|F_L| = \frac{1}{8}\rho R^3 \bar{c}\hat{r}_2^2(S)\left(\frac{d\hat{\phi}}{d\hat{t}}\right)^2 C_L(\alpha)\Phi^2 n^2, \quad \text{(B1)}$$

therefore, the induced roll torque is:

$$L = L_{\text{right}} - L_{\text{left}} \approx \frac{1}{8}\rho R^4 \bar{c}n^2\hat{r}_2^2(S)\hat{r}_{cp}\overline{C_L(\alpha)\left(\frac{d\hat{\phi}}{d\hat{t}}\right)^2\cos(\phi)}\left[(\Phi+\Delta\Phi)^2 - (\Phi-\Delta\Phi)^2\right]$$
$$\approx \frac{1}{2}\rho R^4 \bar{c}n^2\hat{r}_2^2(S)\hat{r}_{cp}\Phi\overline{C_L(\alpha)\left(\frac{d\hat{\phi}}{d\hat{t}}\right)^2\cos(\phi)}\,\Delta\Phi. \quad \text{(B2)}$$

2) Mean stroke angle:

A variation of mean stroke angle $\bar{\Phi}$ (for both left and right wings) will change the instantaneous moment of arm, and result in a pitch moment over one wing stroke (no resultant roll and yaw moment):

$$M \approx 2\overline{F_L}R\hat{r}_{cp}\sin\bar{\Phi} \approx \frac{1}{4}\rho R^4 \bar{c}n^2\hat{r}_2^2(S)\hat{r}_{cp}\overline{C_L(\alpha)\left(\frac{d\hat{\phi}}{d\hat{t}}\right)^2}\Phi^2\sin\bar{\Phi}$$
$$\approx \frac{1}{4}\rho R^4 \bar{c}n^2\hat{r}_2^2(S)\hat{r}_{cp}\overline{C_L(\alpha)\left(\frac{d\hat{\phi}}{d\hat{t}}\right)^2}\Phi^2\bar{\Phi}. \quad \text{(B3)}$$

3) Tilt angle of the stroke plane

A backward tilted left wing stroke plane together with a forward tilted right wing stroke plane will produce a resultant yaw moment over one wing stroke (no resultant roll and pitch moment), which is:

$$\Delta N = 2\left|L_{\text{single wing}}\right| R\hat{r}_{cp}\sin(\Delta\Theta)$$
$$= \frac{2}{8}\rho R^3 \bar{c}\hat{r}_2^2(S)\overline{\left(\frac{d\hat{\phi}}{d\hat{t}}\right)^2 C_L(\alpha)\Phi^2 n^2 R\hat{r}_{cp}}\sin(\Delta\Theta)$$
$$\approx \tfrac{1}{4}\rho R^4 \bar{c}\hat{r}_2^2(S)\hat{r}_{cp}\overline{\left(\frac{d\hat{\phi}}{d\hat{t}}\right)^2 C_L(\alpha)\Phi^2 n^2}\Delta\Theta. \quad \text{(B4)}$$

REFERENCES

[1] M. Sun and Y. Xiong, "Dynamic flight stability of a hovering bumblebee," *Journal of Experimental Biology,* vol. 208, pp. 447-459, Feb 2005.

[2] M. Sun and J. K. Wang, "Flight stabilization control of a hovering model insect," *Journal of Experimental Biology,* vol. 210, pp. 2714-2722, Aug 2007.

[3] G. K. Taylor and A. L. R. Thomas, "Dynamic flight stability in the desert locust Schistocerca gregaria," *Journal of Experimental Biology,* vol. 206, pp. 2803-2829, Aug 2003.

[4] Y. Xiong and M. Sun, "Dynamic flight stability of a bumblebee in forward flight," *Acta Mechanica Sinica,* vol. 24, pp. 25-36, 2008.

[5] Y. Zhang and M. Sun, "Dynamic flight stability of a hovering model insect: lateral motion," *Acta Mechanica Sinica* (available online), 2009.

[6] B. Cheng, "Rotational damping in flapping flight," in *Department of Mechanical Engineering*. Master of Science, Newark: University of Delaware (available online ProQuest/UMI), 2009.

[7] B. Cheng, S. Fry, Q. Huang, and X. Deng, "Aerodynamic damping during rapid flight maneuvers in the fruit fly Drosophila" *Journal of Experiment Biology,* vol. 213, pp. 602-612, 2009.

[8] B. Cheng, S. N. Fry, Q. Huang, W. B. Dickson, M. H. Dickinson, and X. Deng, "Turning Dynamics and Passive Damping in Flapping Flight," in *Proceedings of 2009 IEEE International Conference on Robotics and Automation*, Kobe, Japan, 2009, pp. 1889-1896.

[9] T. L. Hedrick, B. Cheng, and X. Deng, "Wingbeat Time and the Scaling of Passive Rotational Damping in Flapping Flight," *Science,* vol. 324, pp. 252-255, April 10, 2009 2009.

[10] S. N. Fry, R. Sayaman, and M. H. Dickinson, "The aerodynamics of hovering flight in Drosophila," *Journal of Experimental Biology,* vol. 208, pp. 2303-2318, Jun 2005.

[11] R. M. Murray, Z. Li, and S. S. Sastry, *A Mathematical Introduction to Robotic Manipulation*: CRC, 1994.

[12] B. Etkin and L. D. Reid, *Dynamics of Flight: Stability and Control*. New York: Wiley, 1996.

[13] C. P. Ellington, "The Aerodynamics of Hovering Insect Flight .3. Kinematics," *Philosophical Transactions of the Royal Society of London Series B-Biological Sciences,* vol. 305, pp. 41-78, 1984.

[14] S. N. Fry, R. Sayaman, and M. H. Dickinson, "The aerodynamics of free-flight maneuvers in Drosophila," *Science,* vol. 300, pp. 495-498, Apr 2003.

[15] M. H. Dickinson, F. O. Lehmann, and S. P. Sane, "Wing rotation and the aerodynamic basis of insect flight," *Science,* vol. 284, pp. 1954-1960, Jun 1999.

[16] S. P. Sane and M. H. Dickinson, "The aerodynamic effects of wing rotation and a revised quasi-steady model of flapping flight," *Journal of Experimental Biology,* vol. 205, pp. 1087-1096, Apr 2002.

[17] S. P. Sane, "The aerodynamics of insect flight," *Journal of Experimental Biology,* vol. 206, pp. 4191-4208, December 1 2003.

[18] W. B. Dickson and M. H. Dickinson, "The effect of advance ratio on the aerodynamics of revolving wings," *Journal of Experiment Biology,* vol. 207, pp. 4269-4281, November 15 2004.

[19] X. Y. Deng, L. Schenato, and S. S. Sastry, "Flapping flight for biomimetic robotic insects: Part II - Flight control design," *IEEE Transactions on Robotics,* vol. 22, pp. 789-803, Aug 2006.

[20] X. Y. Deng, L. Schenato, W. C. Wu, and S. S. Sastry, "Flapping flight for biomimetic robotic insects: Part I - System modeling," *IEEE Transactions on Robotics,* vol. 22, pp. 776-788, Aug 2006.